doi:10.1016/j.jmb.2010.07.060 J. Mol. Biol. (2010) 402, 669–681

Contents lists available at www.sciencedirect.com

Journal of Molecular Biology

journal homepage: http://ees.elsevier.com.jmb

Influence of the Cytoplasmic Domains of Aquaporin-4 on Water Conduction and Array Formation

Tadanori Mitsuma[1]†, Kazutoshi Tani[1]†, Yoko Hiroaki[1], Akiko Kamegawa[1,2], Hiroshi Suzuki[1,2], Hiroshi Hibino[3], Yoshihisa Kurachi[3] and Yoshinori Fujiyoshi[1,4]*

[1]*Department of Biophysics, Faculty of Science, Kyoto University, Oiwake, Kitashirakawa, Sakyo-ku, Kyoto 606-8502, Japan*
[2]*Japan Biological Informatics Consortium, Oiwake, Kitashirakawa, Sakyo-ku, Kyoto 606-8502, Japan*
[3]*Division of Molecular and Cellular Pharmacology, Department of Pharmacology, Graduate School of Medicine, Osaka University, 2-2 Yamada-oka, Suita, Osaka 565-0871, Japan*
[4]*Biological Information Research Center, National Institute of Advanced Industrial Science and Technology, 2-41-6, Aomi, Koto-ku, Tokyo 135-0064, Japan*

Received 9 June 2010;
received in revised form
24 July 2010;
accepted 28 July 2010
Available online
13 August 2010

Edited by W. Baumeister

Keywords:
water channel;
electron crystallography;
water permeability;
phosphorylation;
orthogonal array

Phosphorylation of Ser180 in cytoplasmic loop D has been shown to reduce the water permeability of aquaporin (AQP) 4, the predominant water channel in the brain. However, when the structure of the S180D mutant (AQP4M23S180D), which was generated to mimic phosphorylated Ser180, was determined to 2.8 Å resolution using electron diffraction patterns, it showed no significant differences from the structure of the wild-type channel. High-resolution density maps usually do not resolve protein regions that are only partially ordered, but these can sometimes be seen in lower-resolution density maps calculated from electron micrographs. We therefore used images of two-dimensional crystals and determined the structure of AQP4M23S180D at 10 Å resolution. The features of the 10-Å density map are consistent with those of the previously determined atomic model; in particular, there were no indications of any obstruction near the cytoplasmic pore entrance. In addition, water conductance measurements, both *in vitro* and *in vivo*, show the same water permeability for wild-type and mutant AQP4M23, suggesting that the S180D mutation neither reduces water conduction through a conformational change nor reduces water conduction by interacting with a protein that would obstruct the cytoplasmic channel entrance. Finally, the 10-Å map shows a cytoplasmic density in between four adjacent tetramers that most likely represents the association of four N termini. This finding supports the critical role of the N terminus of AQP4 in the stabilization of orthogonal arrays, as well as their interference through lipid modification of cysteine residues in the longer N-terminal isoform.

**Corresponding author*. E-mail address: yoshi@em.biophys.kyoto-u.ac.jp.

† T.M. and K.T. contributed equally to this work.

Abbreviations used: AQP, aquaporin; PKC, protein kinase C; 3D, three-dimensional; 2D, two-dimensional; LPR, lipid-to-protein ratio; HEK, human embryonic kidney; FFR, freeze fracture replica; hAQP1, human AQP1.

Introduction

Virtually all living cells have to closely control their water exchange with the environment, which is mediated by transmembrane water channels of the aquaporin (AQP) family.[1,2] Most AQPs are thought to be in a constitutively open channel conformation, but the permeability of some water channels is regulated by various mechanisms.[3] For instance, gating of the functionally and structurally well-studied plant water channel PIP2 is thought to protect plants against draught or flood.[4,5] The water permeability of mammalian AQP0 is regulated both by pH, at least partially due to the protonation state of a His residue in loop A, and by Ca^{2+} in a calmodulin-dependent gating mechanism.[3,6] All these mechanisms regulate AQPs in response to environmental conditions and are closely related to the physiological functions of the cells expressing the water channels.

While also expressed in other organs, AQP4 is the predominant water channel in the brain. AQP4 forms distinct crystalline arrays at the end feet of astrocytes, which are known as orthogonal arrays.[7,8] The size of these orthogonal arrays is determined by the ratio at which two AQP4 splicing isoforms are expressed.[9] The N terminus of the full-length protein starting with Met1 (AQP4M1) contains lipid-modified cysteine residues and thus interferes with array formation. In contrast, the short AQP4 isoform starting with Met23 (AQP4M23) can form arrays because it lacks the lipid-modified cysteine residues in the N terminus.[10] It remains elusive, however, why AQP4 forms arrays.

Protein kinase C (PKC) was shown to reduce the water permeability of AQP4 in astrocytes by phosphorylating it in a dopamine-dependent manner.[11] When Ser180 in loop D was mutated to alanine, PKC no longer affected the water permeability of AQP4, suggesting Ser180 as the residue that is phosphorylated by PKC.[11,12] Protein kinase G increases the water permeability of AQP4 by phosphorylating Ser111 in loop B.[13,14] Furthermore, expression of an S111D mutant in LLC-Pk1 cells showed that it forms larger arrays compared to wild-type AQP4.[15] Phosphorylation of the C terminus of AQP4 has no effect on the water permeability, but was shown to enhance the cell surface expression of AQP4.[16] In addition to water conduction, AQP4 was recently shown to have other essential roles in brain homeostasis. AQP4 regulates K^+ uptake into synapses, and loss of AQP4 inhibits the proliferation, survival, migration, and neuronal differentiation of adult neural stem cells.[17] Its varied physiological roles may explain why AQP4 has been implicated in several brain pathologies, including brain edema[18] and neuromyelitis optica.[19]

To examine the structural effect of phosphorylation, we expressed AQP4 carrying an S180D mutation (designed to mimic the phosphorylated state of Ser180) and determined its structure by electron crystallography at 2.8 Å resolution.[20] The mutation of serine residues located in consensus phosphorylation sites to a negatively charged aspartate or glutamate residue is a method that is commonly used to mimic its phosphorylated state. Although PKC-dependent phosphorylation of Ser180 reduced the water conduction of AQP4 by half,[11] the structure of the S180D mutant did not show significant conformational changes compared to the structure of wild-type AQP4.[20,21] The atomic structure of the S180D mutant thus provided no insights into the mechanism by which phosphorylation of Ser180 reduces the water permeability of AQP4.

Discrepancies between structural and functional studies can result when the crystallization conditions induce or stabilize a nonphysiological conformation of the protein. For example, while functional assays showed the yeast water channel Aqy1 to conduct water, in the crystal structure, the N terminus closed the channel by obstructing the entrance.[22] Furthermore, low-resolution density maps obtained from three-dimensional (3D) reconstruction based on electron micrographs of two-dimensional (2D) crystals can reveal protein domains that are partially disordered and usually not resolved in high-resolution maps.[23,24] Therefore, to investigate the structural and functional effects of phosphorylation on Ser180, we calculated a density map from images of the 2D crystals of the S180D mutant designed to mimic phosphorylation and studied its water conduction *in vitro* and *in vivo*.

Results

The water channel in AQP4M23S180D is in an open conformation

Phosphorylation of Ser180 by PKC has been implicated in the regulation of AQP4 water permeability.[11] To visualize any potential conformational changes that may result from its phosphorylation, we mutated Ser180 in rat AQP4M23 to Asp (AQP4M23S180D) to mimic its phosphorylated state. The recently determined structure of this mutant at 2.8 Å resolution showed, however, that it was essentially identical with that of the wild-type protein.[20] The root-mean-square deviation between the backbone atoms of the S180D mutant and those of rat wild-type protein[21] is 0.77 Å, and that between the mutant and the human wild-type protein is 0.61 Å.[25] These structural comparisons demonstrate that the S180D mutation does not induce large conformational changes in AQP4 structure. To further compare the pore structure

of AQP4M23S180D with those of wild-type AQP4M23 and other AQPs, we used the program HOLE[26] to calculate pore profiles (Fig. 1). As previously shown, the pore profile of PIP2;1 in the closed conformation confirms that the cytoplasmic side of the channel is too narrow to allow water conduction.[4] By contrast, the pore profiles indicate that the cytoplasmic side of the channel is wider in the S180D mutant than in wild-type AQP4. In conclusion, the 2.8-Å structure of AQP4M23S180D does not support the notion that phosphorylation of Ser180 would induce the water channel to adopt a closed conformation.

Analysis of the AQP4M23S180D structure based on image data

Low-resolution density maps calculated from cryo electron micrographs sometimes show partially ordered regions of a protein that are not resolved in high-resolution maps.[23,24] We therefore collected images of AQP4M23S180D 2D crystals and used them to calculate a 3D reconstruction at 10 Å resolution (Table 1, Fig. 2). The features of the density map were completely consistent with the previously determined atomic model of AQP4M23S180D.[20] In particular, the 10-Å map did not reveal any density that could obstruct the channel entrance and thus potentially reduce water permeability (Fig. 3a). Furthermore, although loop D carrying Asp180 was not clearly resolved as a result of the low resolution of the map, the density nicely accommodated the atomic model, which did not have to be modified to fit the density (Fig. 3a). The 10-Å density map calculated from image data thus further supports the conclusions from the atomic model that the water channel in AQP4M23S180D is in an open conformation and that phosphorylation of Ser180 does not induce conformational changes in AQP4 that would reduce its water permeability.

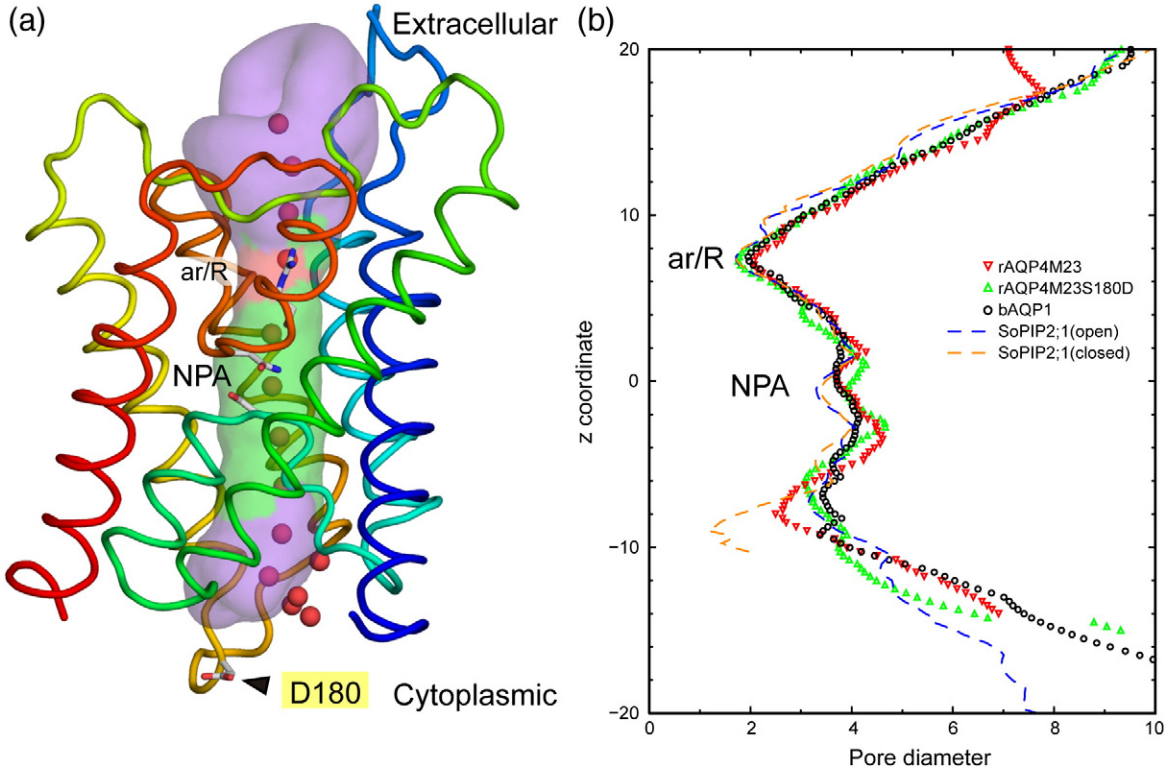

Fig. 1. The water channel in AQP4. (a) The translucent surface shows the boundary of the water channel as calculated by HOLE.[26] The color of the surface represents the pore diameter: red, narrow (constricted region; ar/R); green, intermediate (NPA motif conserved in AQPs; NPA); purple, wide (pore entrances). AQP4, shown in tube representation, is shown from blue (N terminus) to red (C terminus). Residue 180, the position of the S180D mutation, and residues at ar/R and NPA are shown in stick representations. Waters in the channel are shown as red spheres. (b) Pore profiles of rat AQP4M23 (rAQP4M23),[21] rat AQP4M23S180D (rAQP4M23S180D),[20] bovine AQP1 (bAQP1),[27] and spinach PIP2;1 (SoPIP2;1) in the open and closed conformations,[4] as calculated by HOLE.[26] The diameter of the narrowest region of the PIP2;1 channel in the closed conformation is about 1 Å, while the narrowest region of water channels in the open conformation is the ar/R constriction site, with a diameter of about 2 Å.

Table 1. Electron crystallographic data

2D crystal	
Space group	$P42_12$
Lattice constants	$a=69.0$ Å, $b=69.0$ Å, $c=160.0$ Å (assumed), $\gamma=90.0°$
Number of images used at approximate tilt angle	
0°	9
20°	44
45°	84
60°	109
Total	246
Resolution limit	
In-membrane plane (Å)	10.0
Normal-to-membrane plane (Å)	10.9
Range of underfocus (Å)	4300–37,300
Number of observed reflections	7903
Number of independent reflections	230
Overall weighted phase residuals[a]	26.5
Overall weighted *R*-factor[a]	0.4314

[a] Used reflections are better than IQ[28] 6.

The 10-Å map shows an interesting feature—a density on the cytoplasmic side that connects four adjacent tetramers (Fig. 3). Based on the docked crystal structure, this density likely represents the N terminus of AQP4M23, and the interaction of N termini from the subunits of four adjacent tetramers suggests a direct role of the N terminus in forming and/or stabilizing a 2D array. The same feature could already be seen in the density map of wild-type AQP4M23 obtained from image data contoured at 0.8σ, but it was not discussed because it was close to the noise level. The larger number of images (246) used to calculate the 3D reconstruction of the mutant (Table 1)—as compared to 135 images used to obtain the density map of wild-type AQP4M23[21]—improved the signal-to-noise ratio of the data set. As a result, the density created by the connecting N termini is clearly seen even if the density map is displayed at a contour level of 0.65σ (Fig. 3). Although weaker in the map of the wild-type protein, the corresponding density was identical with that seen in the map of the mutant. Their clear density at the limited resolution of our map leads us to propose that the N termini are directly involved in array formation. However, the N termini of both wild-type AQP4M23 and S180D mutant have a length of 39 amino acid residues, which include a 6×His tag and a linker sequence. Furthermore, the density between the tetramers was only visible in the low-resolution map, suggesting that the protein is partially disordered in this region. We can therefore not exclude the possibility that the density represents the N-terminal His tag and/or linker sequence.

Measurement of water permeability *in vitro*

To further confirm that the water channel in the S180D mutant is in an open conformation, we used an *in vitro* assay (described in Reconstitution of Recombinant AQPs into Liposomes for Functional Assay) to measure the water permeability of AQP4M23S180D reconstituted into lipid vesicles. Because the absolute rate of water permeation cannot be measured very accurately, we also measured the water permeation of wild-type AQP4 for comparison with that of the S180D mutant. In addition, we also measured the water permeability of empty liposomes, to obtain the basal water permeability of the lipid bilayer, and the water permeability of AQP1 proteoliposomes, as AQP1 is one of the fastest water channels.

We first measured proteoliposomes obtained at a lipid-to-protein ratio (LPR) of 100 (wt/wt) and found that the water permeation rate (P_f; in cm/s) of AQP4M23S180D is $5.84\pm0.22\times10^{-3}$ ($N=65$), which is lower than that of AQP1 ($7.22\pm0.39\times10^{-3}$; $N=65$) but higher than that of wild-type AQP4M23 ($3.65\pm0.15\times10^{-3}$; $N=68$) (Fig. 4a). To further increase the reliability of our results, we measured proteoliposomes produced at LPRs ranging from 75 to 250. All measurements showed the same tendency, with AQP1 displaying the highest water conduction rate, followed by AQP4M23S180D, and with wild-type AQP4M23 displaying the lowest water conduction rate (Fig. 4b). Since all measurements consistently showed that the water permeability of AQP4M23S180D is higher than that of wild-type AQP4M23, these results corroborate the open conformation of the water channel seen in the structure of AQP4M23S180D, but are not consistent with the initial observation that phosphorylation of Ser180 decreases water conduction by AQP4.[11]

Measurement of water permeability *in vivo*

In addition to our *in vitro* assay, we also measured the water permeability of wild-type and S180D mutant AQP4M23 expressed in human embryonic kidney (HEK) 293T cells (see Cell Volume Assays). Transfected HEK293T cells loaded with calcein fluorescence were alternatively perfused with isotonic and hypotonic buffers, and water permeability was deduced from changes in cell volume and fluorescence (Fig. 5a–c). We then determined the time constant τ describing the time-dependent decrease in fluorescence intensity as a result of the exchange of isotonic buffer and hypotonic buffer, as well as the maximum reduction in fluorescence intensity (the difference between the intensity at the beginning of the experiment and the intensity after hypoosmotic shock). We found that the increase in the water permeability of cells transfected with AQP4M23S180D was identical with the increase in the water permeability of cells transfected with wild-type AQP4M23, which was about ~14-fold higher than the water permeability of mock-

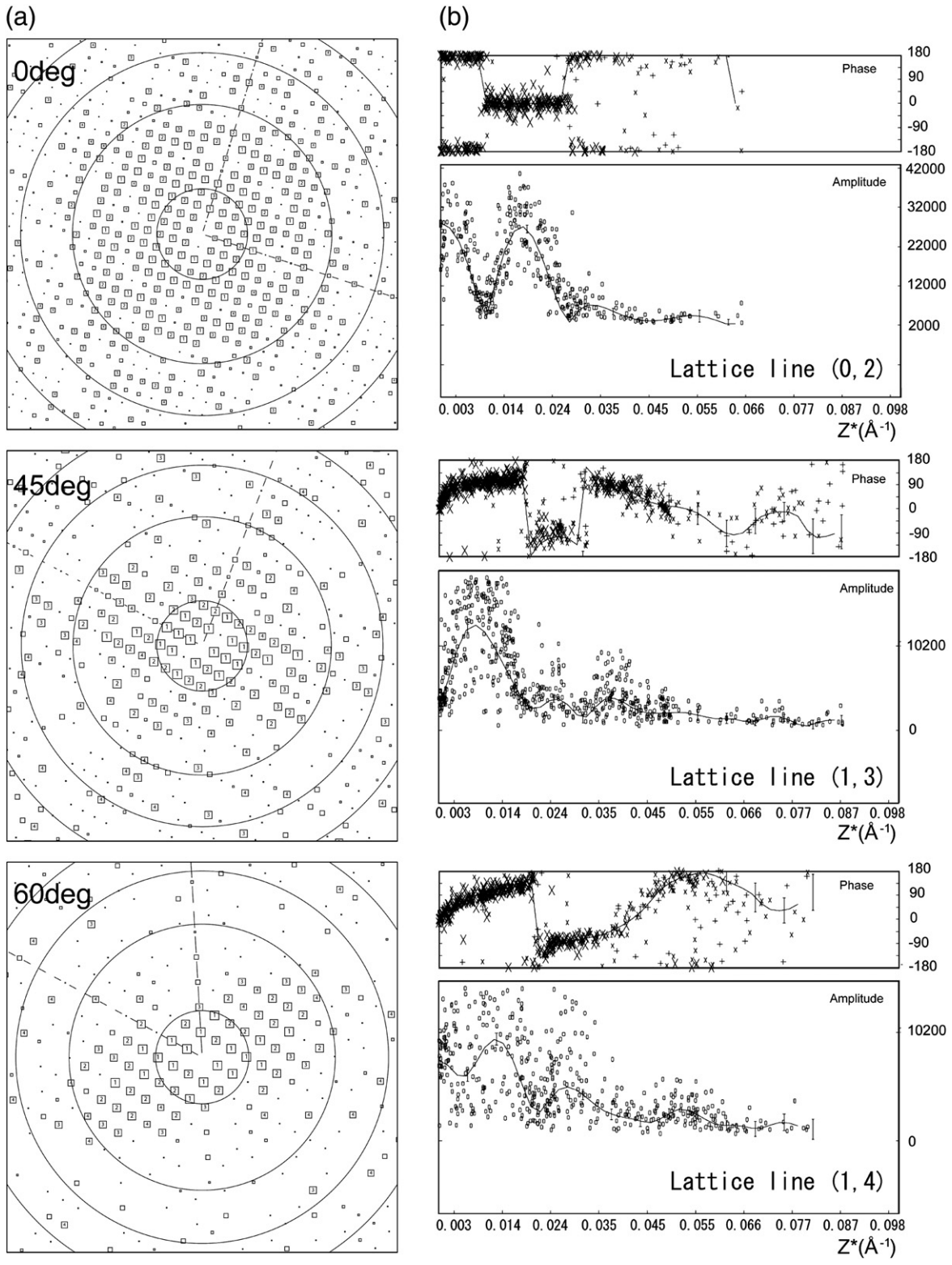

Fig. 2. IQ plots and lattice lines. (a) IQ[28] plots calculated from Fourier transforms of the frozen–hydrated trehalose-embedded 2D crystals of AQP4M23S180D. Circles indicate resolutions of 20 Å, 7 Å, 5 Å, and 4 Å. (b) Representative lattice lines (0, 2), (1, 3), and (1, 4) showing a good match between experimental data and the fitted curve. The measured phases for lattice line (0, 2) were mostly 0° or 180°, consistent with the $P42_12$ symmetry of the AQP4M23S180D crystals.

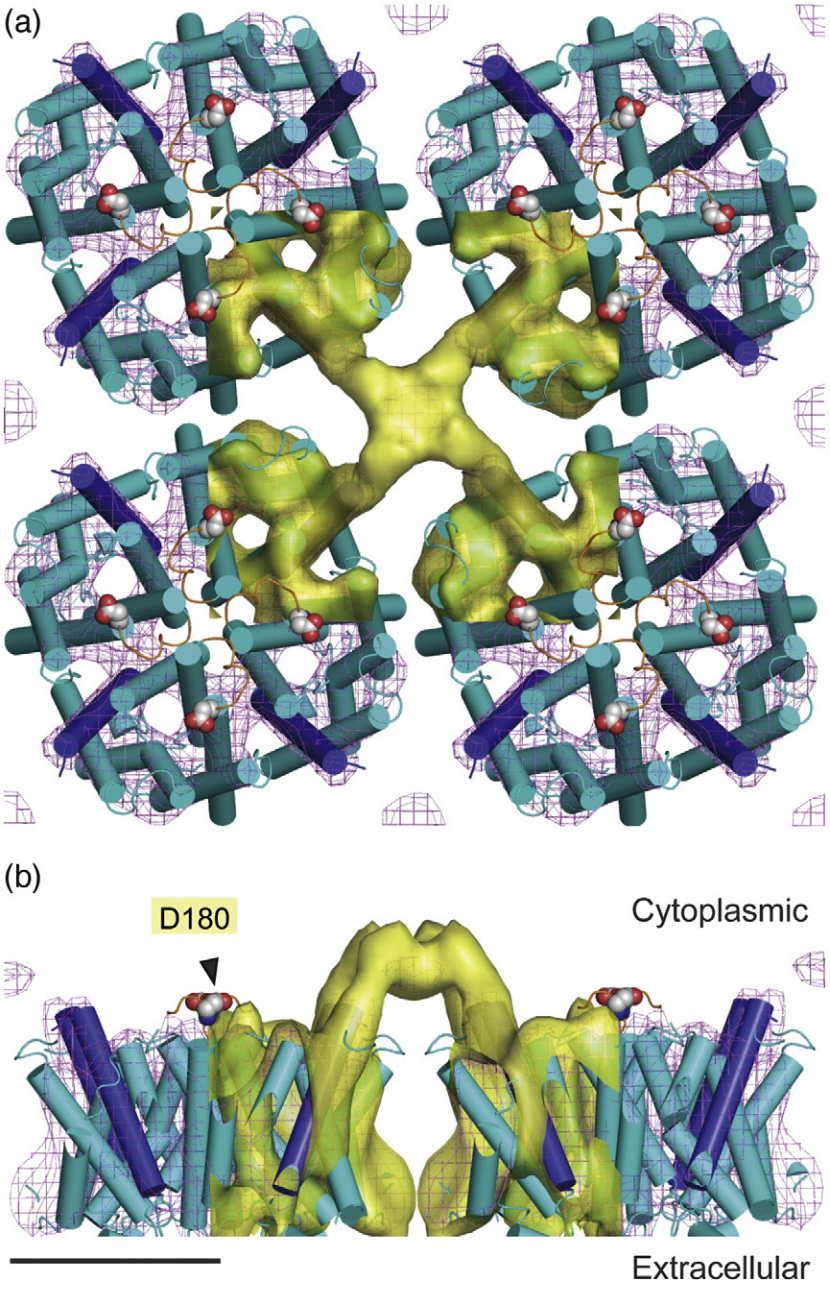

Fig. 3. Atomic model of AQP4M23 and the 10-Å 3D map calculated from electron micrographs viewed from the cytoplasmic side (a) and parallel with the membrane (b). Even at a contour level of 0.65σ (yellow surface), the density map was essentially free of noise. The map also represented by violet mesh was contoured at 1.0σ and clearly showed the N-terminal first transmembrane helix (blue cylinder). The density map shows no obstructions of the pore entrance, but a prominent density on the cytoplasmic side that connects four adjacent tetramers, and is likely to represent the N terminus. The α-helices of AQP4M23 are shown as cylinders, and residue D180 in loop D (orange loop) is shown in sphere representation. Scale bar represents 35 Å.

transfected cells (Fig. 5d). In addition, we did not find significant differences in the maximum change in fluorescence intensity between mock-transfected cells (13.38±0.33%; $N=38$) and cells transfected with wild-type AQP4M23 (12.77±0.33%; $N=30$) or AQP4M23S180D (13.10±0.38%; $N=33$) (Fig. 5e). Four repetitions on different days with different cells produced similar results. Together with the comparable expression levels of wild-type AQP4M23 and AQP4M23S180D (Fig. 6), the results of the *in vivo* measurements are fully consistent with those obtained with the *in vitro* assay.

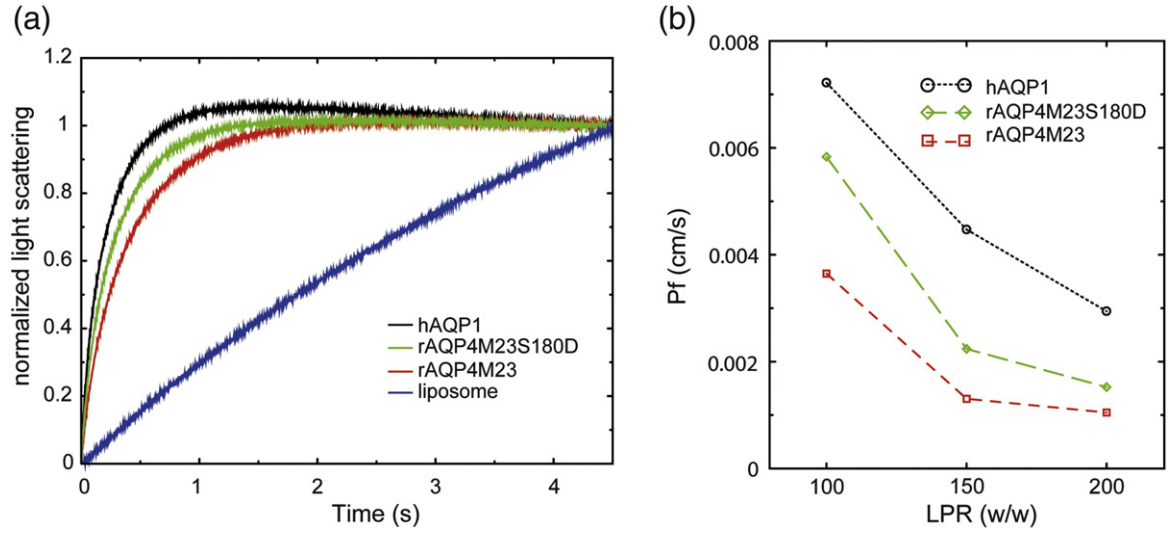

Fig. 4. Water permeability of AQPs reconstituted into proteoliposomes. (a) Stopped-flow measurements of water conduction by empty liposomes and AQP proteoliposomes reconstituted at LPR=100. hAQP1 shows the highest water permeability, followed by rAQP4M23S180D and rAQP4M23. (b) Graph of water permeability as a function of the LPR of the proteoliposomes. Regardless of the LPR, the water conduction rate of the S180D mutant was consistently higher than that of wild-type AQP4M23.

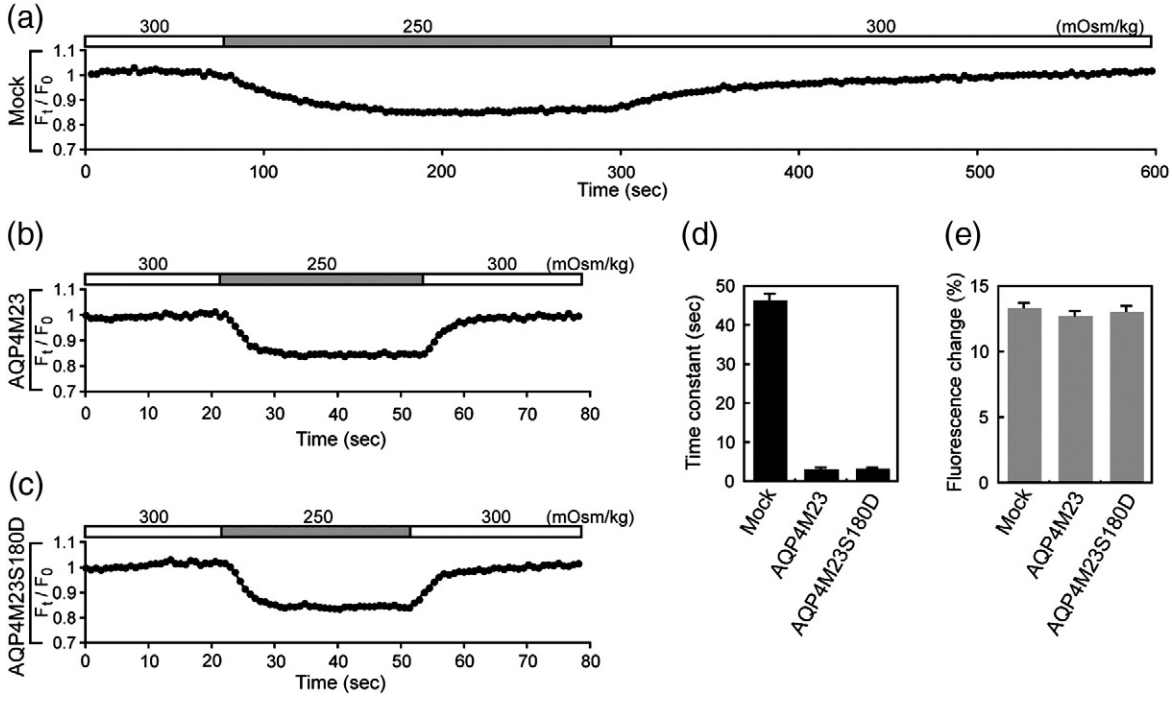

Fig. 5. Water permeability of wild-type and S180D mutant AQP4M23 measured in transfected HEK293T cells. (a–c) Water permeability measured as a change in the cell volume of calcein-loaded HEK293T cells transfected with (a) empty plasmid, (b) AQP4M23, or (c) AQP4M23S180D. Cells were exposed to an isotonic solution (300 mOsm/kg) and a hypotonic solution (250 mOsm/kg), and their fluorescence was measured by confocal light microscopy. (d) Time constants describing the decrease in fluorescence for control cells (Mock; $n=38$), cells expressing wild-type AQP4M23 (AQP4M23; $n=30$), and cells expressing the S180D mutant (AQP4M23S180D; $n=33$). (e) Maximum change in fluorescence intensity, which was measured as the difference between the intensity at the beginning of the experiment and the intensity at the end of hypotonic shock. The numbers of measurements are the same as in (d).

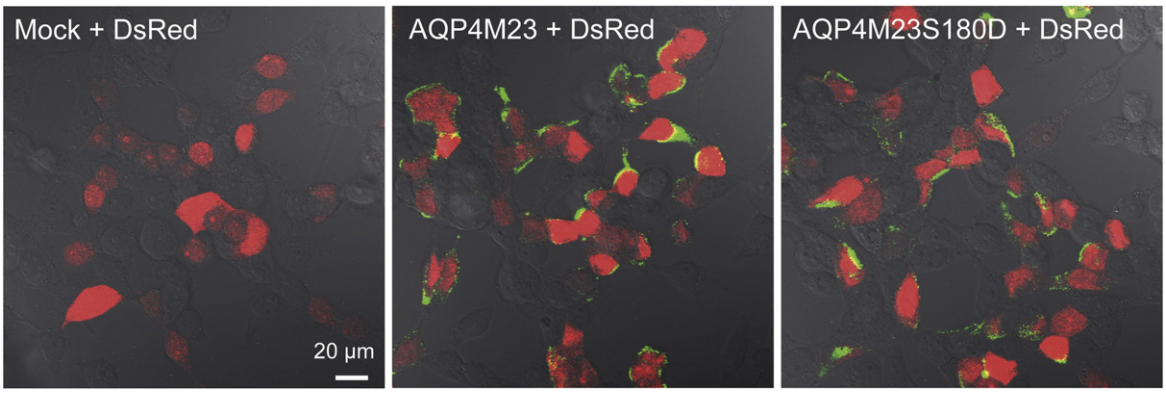

Fig. 6. Immunolabeling of HEK293T cells to determine the percentage of cells expressing AQP4. Cells were transfected with empty pcDNA3.1 plasmid (Mock) or with pcDNA3.1 containing cDNA for AQP4M23 or AQP4M23S180D, and simultaneously transfected with DsRed monomer plasmid. The transfected cells were incubated with anti-AQP4 antibodies and then treated with Alexa488-conjugated secondary antibody.

In conclusion, all our experimental results (from structural studies and from water permeability measurements *in vitro* and *in vivo*) strongly suggest that the S180D mutation, mimicking phosphorylation of this residue, does not reduce water conduction by AQP4.

Discussion

Potential role of loop D in the regulation of AQP4 water conduction

To address the physiological relevance of the phosphorylation of Ser180 in loop D, we examined the effect of the S180D mutation thought to mimic the phosphorylation of this residue. All our *in vitro* and *in vivo* functional assays showed that the S180D mutation does not reduce water conduction by AQP4, and our results are thus not consistent with the previous finding that phosphorylation of S180 reduces the water permeability of AQP4 to half the value of the unphosphorylated protein.[11]

It is well known that physiological effects resulting from the phosphorylation of a serine or threonine residue, such as conformational changes in the protein, cannot always be reproduced by substituting the residue with a negatively charged glutamate or aspartate residue. For example, neither the phosphorylation of PIP2;1[29] nor the phosphorylation of CDK2[30] could be mimicked by substituting the phosphorylated residue with a negatively charged residue. Phosphorylation of a residue introduces two negative charges, whereas mutation to glutamate or aspartate introduces only a single negative charge. This difference in charge results in the distinguished conformational change, which can be observed both in experiments and in simulations, in between the phosphorylated version and the mutated version of the protein having different energy landscapes.[31,32]

Even though subunits may be in equivalent positions in a crystal, individual subunits can potentially take independent structures in their multimeric structure. For example, the first crystals of the bacterial transporter AcrB had a trigonal *R*32 symmetry, in which all subunits in the trimer are related by a crystallographic 3-fold symmetry axis,[33] but later crystals had a *C*2 symmetry, in which each subunit of the trimer is independent of the others.[34] Furthermore, the phosphorylation rate in the cytoplasm is low, and it is unlikely that all four Ser180 residues in the AQP4 tetramer are phosphorylated. Thus, mimicking phosphorylation by the S180D mutation may force all subunits into the same conformation and potentially prevent the tetramer from adopting a physiologically relevant asymmetric structure.

Although the structure of AQP4M23S180D did not reveal significant differences from the structure of the wild-type protein, the results of our *in vitro* assay consistently showed the mutant to have a higher water permeability. This higher water permeability may possibly be due to the additional negative charge introduced by the S180D mutation, which, together with Asp184, creates a significant negative charge at the center of the tetramer. Interestingly, SDS-PAGE analysis of the purified proteins showed that AQP4M23S180D runs as a mixture of monomer and dimer species, whereas wild-type AQP4M23 and AQP1 run exclusively as monomers (Fig. 7a). This result suggests that the S180D mutation causes stronger interactions between AQP4 subunits. Loop D of one subunit makes van der Waals contacts and forms hydrogen bonds with loop B of an adjacent subunit (Fig. 7b), thus potentially stabilizing dimer interactions and, by

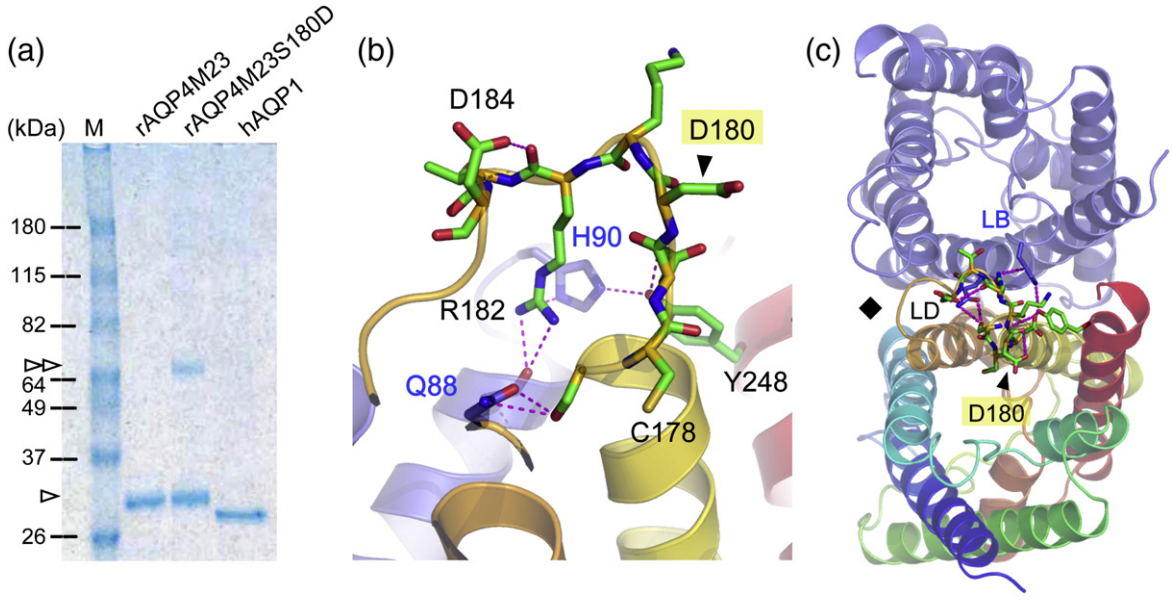

Fig. 7. Stabilization of the AQP4 oligomer. (a) SDS-PAGE analysis of AQPs. Unlike wild-type AQP4M23, a fraction of AQP4M23S180D runs as a dimer. (b and c) Side view (b) and view from the cytoplasmic side (c) of the hydrogen bonds (dotted lines) and van der Waals interactions between loop D of one subunit [blue (N terminus) to red (C terminus)] and the N-terminal region of the loop B of the adjacent subunit (in purple, including residues Q88 and H90). Residues C178-G185, as well as hydrogen-bond donors and acceptors, are shown as stick models.

extension, tetramer organization (Fig. 7c). Since loop B is located close to the water pore, changes in the interaction of loop D with loop B could thus influence the water permeability of AQP4. In summary, the S180D mutation may increase the water permeability of AQP4 by changing the interaction of loop D with loop B, which also manifests in a strengthening of subunit interactions.

Other studies have already implicated loop D in changes in the water permeability of AQP4. For example, binding of a mercury ion to cysteine 178 reduced water conduction of AQP4 in a fully reversible manner.[35] Structural and mutational studies of *Escherichia coli* AQPZ showed that mercury can reversibly inhibit water conduction by binding to a pore-facing cysteine residue, thus blocking the water channel.[36] As C178 in AQP4 does not extend into the water channel, mercury has to affect water conduction by AQP4 by a different mechanism. Another example is the mutation of aspartate 184 to glutamate, which decreases the water permeability of AQP4.[37] Since residues C178, S180, and D184 are all located in loop D (Fig. 7b), the conformation of loop D appears to affect the water permeability of AQP4, likely through its interaction with loop B. A full understanding of how phosphorylation of Ser180 increases water permeability will require structures of both the phosphorylated protein and the unphosphorylated protein at a resolution of at least 3 Å. Nevertheless, the current study shows that the water permeability of AQPs appears to be affected by the organization of cytoplasmic loops.

Potential role of the N terminus in orthogonal array formation

Our 10-Å density map clearly resolves a density at the cytoplasmic surface that connects four adjacent tetramers and is most likely formed by the N terminus of AQP4. We cannot be sure, however, that this connecting density exists in native orthogonal arrays in astrocytes, since our AQP4 construct contains 39 additional N-terminal residues that include a His tag and a linker sequence. The position of the connecting density in the low-resolution map is consistent with the N terminus, but it was not present in the high-resolution map calculated with intensities from electron diffraction patterns and phases obtained by molecular replacement.[20] We cannot exclude the possibility that the connecting density would also be visible in higher-resolution density maps if experimental phases from high-resolution images would be used; however, we think this to be unlikely because the previous 2.8-Å map allowed us to model not only the structure of AQP4 but also the structures of several lipids and water molecules.

The volume of the density connecting four adjacent tetramers is 3312 $Å^3$ when contoured at 0.65σ (Fig. 3). Thus, the volume for each AQP4M23S180D monomer that is not accounted

for by the atomic model is 828 Å^3, corresponding to about six amino acids, assuming a density of 0.81 Da/Å^3.[38] Although only a rough estimate, as the volume included in a density map strongly depends on the chosen contouring level, the deduced number of residues seems to be consistent with the N-terminal cytoplasmic region (M23-V29) missing from the AQP4M23S180D model. Therefore, additional N-terminal His-tag linker sequences are still unresolved both in the 10-Å-resolution map and in the atomic-resolution map. Interestingly, recent studies using single quantum dot observations of cells expressing AQP4M23 reported that mutants with deletions or additions to the N terminus failed to form arrays.[39,40] Moreover, replacing the N-terminal domain of AQP1 with that of AQP4M23 was sufficient to induce AQP1 to form arrays.[40] Arrays of AQP4M23 are stabilized by hydrophobic interactions between the N termini of adjacent tetramers. These interactions are nonselectively blocked by seven residues just upstream of the N terminus of AQP4M23, preventing the longer AQP4M1 isoform from forming arrays. These findings are in agreement with our previous results obtained with the freeze fracture replica (FFR) method, which showed that AQP4 mutants starting at residue 17 or residue 18 (M17 or M18, respectively) inhibit array formation.[10] Furthermore, the inhibition of array formation by the palmitoylation of the AQP4M1 N terminus, which is overcome by ablating palmitoylation sites,[10] suggests that the distance of the N terminus from the membrane may be critical for the inhibition mechanism.

Crane and Verkman reported that the deletion of four N-terminal residues decreased to 20–30% of the forming arrays of AQP4,[40] but our previous FFR experiments showed that the same deletion mutant had a normal efficiency of forming arrays like wild type.[10] These contradictory results could possibly be explained by the temperature-dependent manner of AQP4 array formation, since the double mutant AQP4M1-C13A/C17A could not form AQP4 arrays above 37 °C, but they could make array formation under 10 °C, as in our previous FFR results.[41] Nevertheless, despite the two different expression systems used, in both cases, array formation by AQP4 appears to be affected by modifications to the N-terminal residues of AQP4M23. A recent study showed that array formation does not occur in the endoplasmic reticulum membrane just after AQP4 synthesis, but that the first arrays are formed in the trans-Golgi membrane.[42] In consideration of all these results and our finding that array formation is prevented by the palmitoylation of the N terminus,[10] array formation by AQP4 appears to be regulated by several mechanisms. Further structural and functional studies are needed to resolve the biological properties of array formation by AQP4.

Materials and Methods

Three-dimensional reconstruction from images of 2D crystals

The electron micrographs used in this study are those that were previously used to determine the 2.8-Å structure of AQP4M23S180D.[20]

All digitized images were processed with a modified version of MRC image processing programs.[43] Images were computationally unbent and corrected for contrast transfer function.[28] The initial contrast transfer function parameters for each image were determined using CTFPro.[20,44] Despite suffering from radiation damage (specimens were exposed twice, first to record a diffraction pattern and then to collect the image[20]), the Fourier transform of each image diffracted beyond 7 Å resolution along the tilt axis (Fig. 2). Images from crystals belonging to the predominant crystal type ($P42_12$) were merged and used to calculate a 3D density map at 10 Å resolution (Fig. 2). The statistics of our electron crystallographic structure of AQP4M23S180D are summarized in Table 1. Figures 1a, 3, and 7b were prepared with PyMOL‡.

Reconstitution of recombinant AQPs into liposomes for functional assay

Reconstitution was performed as described previously, with some modifications.[45,46] cDNAs encoding rat AQP4M23 and AQP4M23S180D were subcloned into pBlueBacHis2B (Invitrogen Corp., Carlsbad, CA, USA). cDNA encoding human AQP1 (hAQP1) was subcloned into pAcHLT-A (BD Biosciences). The constructs were verified by restriction enzyme digestion and DNA sequencing, and plasmid DNA was purified with the Qiagen plasmid maxi kit. Recombinant AQP4 baculovirus was prepared with the Bac-N-Blue transfection kit (Invitrogen Corp.). Recombinant AQP1 baculovirus was prepared with the BaculoGold transfection kit (BD Bioscience). AQP4 and AQP1 were expressed in Sf9 insect cells,[21] membranes were prepared,[47] and proteins were purified.[21] Proteins were reconstituted into liposomes, as described previously.[48] Briefly, 50 μg of purified protein was mixed with 5 mg of dimyristoylphosphatidylcholine (Sigma-Aldrich) in 2% *n*-octyl-β-D-glucopyranoside and incubated for 20 min at 22 °C. Proteoliposomes (or control liposomes without protein) were formed by rapidly injecting the solution into detergent-free buffer [50 mM Hepes (pH 7.5) and 0.5 mM PMSF] at 22 °C. The suspension was incubated for 20 min at 22 °C and centrifuged at 123,000*g* for 1 h. The pellet was resuspended in the same buffer and centrifuged at 140,000*g* for 1 h. Proteoliposomes (or empty liposomes) were resuspended in 1 ml of the same buffer. All centrifugations were performed at 4 °C. The proper insertion of AQP into the liposomes was verified by Western blot analysis with anti-AQP1 or anti-AQP4 antibodies (CHEMICON, Temecula, CA, USA), respectively.

‡ http://pymol.sourceforge.net/

Measurement of water permeability by stopped-flow light scattering

Water permeability in proteoliposomes containing AQP4M23, AQP4M23S180D, or hAQP1 was measured by stopped-flow light scattering, as previously described,[45,46] with modification [the average size of the proteoliposomes was determined by dynamic light scattering using an ELSZ-0 instrument (Otsuka Electronics, Japan) or an N4 Sub-Micro Particle Analyzer (Beckman Coulter, Fullerton, CA, USA)]. Proteoliposomes or empty liposomes were equilibrated for 1 h at 22 °C to reach isothermal conditions. Measurements were carried out with an SX20 stopped-flow spectrometer (Applied Photophysics). Vesicles were subjected to a 100 mM inwardly directed sucrose gradient at 22 °C, and the kinetics of vesicle shrinkage were measured by recording over time the change in intensity of 90° scattered light at a wavelength of 450 nm. Time courses were normalized at 10 s and fitted to single-exponential curves to determine the velocity constant k (s^{-1}). Osmotic water permeability coefficients (P_f) were calculated as described previously.[49] Since the amount of protein in the proteoliposomes was too small to be accurately measured with the DC protein assay kit (Bio-Rad), the theoretical LPR of the proteoliposome was used for the calculations in this study.

Cell volume assays

Cell volumes were determined as described previously.[50–52] HEK293T cells were transfected by FuGene (Roche) with 0.4 μg of either AQP4-M23wt-pcDNA3.1, AQP4-M23S180D-pcDNA3.1, or pcDNA3.1 (mock; Invitrogen Corp.), plus 1.6 μg of DsRed monomer plasmid (Clontech). The transfected cells were incubated for 2 days at 37 °C.

After a wash with serum-free Dulbecco's modified Eagle's medium, cells were loaded with 1 μM calcein–acetoxymethyl ester (Invitrogen Corp.) in serum-free Dulbecco's modified Eagle's medium for 20 min at 37 °C and immediately used for water conduction assays. Cells were imaged with a confocal microscope (LSM-510, 40× oil objective, numerical aperture of 1.3, room temperature; Carl Zeiss, Jena, Germany) using an excitation wavelength of 488 nm and an emission wavelength of 505–530 nm. The fluorescence intensity was measured as the average of the signals in regions of interest, which included, whenever possible, the entire area of a cell in a section. Measurements were taken every 786.43 ms (which was the minimum duration under our experimental conditions) for cells expressing wild-type and mutant AQP4, and taken every 3 s for control cells (to minimize photobleaching). To account for photobleaching, we corrected the fluorescence for each cell using either the linear slope or the exponential curve for images taken at the beginning and at the end of each experiment,[52] when the cells were exposed to isotonic solution (Fig. 5). For cells expressing wild-type or mutant AQP4, the first 25 images and the last 15 images were used for correction; for control cells, the first 25 images and the last 10 images were used.

The osmolarity of the buffer solution was recorded with an osmometer (OM802; Vogel, Kevelaer, Germany) and adjusted to 300 mOsm/kg for isotonic conditions and to 250 mOsm/kg for hypotonic conditions by adding mannitol to a buffer solution consisting of 5.5 mM Hepes–NaOH (pH 7.4), 100 mM NaCl, 5 mM KCl, 1.8 mM $CaCl_2$, 0.53 mM $MgCl_2$, and 5.5 mM glucose. Cells were continuously perfused by gravity with buffer solution at a rate of 10 ml/min. We verified that in transfections with wild-type and mutant AQP4, >90% of the cells displaying red fluorescence showed a rapid decrease in calcein fluorescence upon hypoosmotic shock (data not shown).

HEK293T cells were immunolabeled as described previously.[52] Cells transfected with cDNAs for AQP4-M23-pcDNA3.1, AQP4-M23S180D-pcDNA3.1, or pcDNA3.1 (mock) were incubated for 2 days, fixed with 4% paraformaldehyde in 100 mM sodium phosphate (pH 7.4) at 4 °C overnight, and then washed twice with phosphate-buffered saline for 10 min. Samples were treated with 1% bovine serum albumin in phosphate-buffered saline containing 0.1% Triton X-100 for 30 min, incubated with anti-AQP4 antibodies (Almone Labs, Jerusalem, Israel) at 4 °C overnight, and then incubated with Alexa488-conjugated secondary antibodies (Invitrogen Corp.) at room temperature for 2 h. Based on the number of cells displaying the fluorescence of DsRed, 91% of cells expressed AQP4M23 (103 of 113 cells), and 88% of cells expressed AQP4M23S180D (79 of 89 cells). Finally, green fluorescence and red fluorescence were examined with a confocal microscope.

SDS-PAGE

For SDS-PAGE analysis, samples were run on 10–20% polyacrylamide gradient gels (Wako), and gels were stained with Simply Blue SafeStain (Invitrogen Corp.). In order to adjust the total amount of proteins in each lane, we determined protein concentrations using UV absorption at 280 nm.

Accession numbers

The cryo-EM density map of AQP4M23S180D has been deposited in the Electron Microscopy Data Bank§ with accession code EMD-5202. The coordinates and structure factors of AQP4M23S180D have been deposited in the Protein Data Bank with accession code 3IYZ.

Acknowledgements

We acknowledge Drs. K. Abe and T. Doi for discussions, Dr. M. Yasui for access to the Particle Analyzer, and Mr. K. Kobayashi (JEOL DATUM) for technical assistance. We thank Dr. T. Walz for critical reading of the manuscript. This work was supported by Grant-in-Aid for Young Scientists (B) 22770147 (to K.T.); Grant-in-Aid for Scientific Research on Priority Areas 17081012 (to H.H.); Grant for 'Research and Development of Next-

§ http://www.emdatabank.org/

Generation Integrated Life Simulation Software' (to Y.K.); Grant-in-Aid for Scientific Research (S) (to Y.F.); the Global COE Program A06 to Kyoto University (to Y.F.) from the Ministry of Education, Culture, Sport, Science, and Technology of Japan; and the Japan New Energy and Industrial Technology Development Organization (to Y.F.).

References

1. Borgnia, M., Nielsen, S., Engel, A. & Agre, P. (1999). Cellular and molecular biology of the aquaporin water channels. *Annu. Rev. Biochem.* **68**, 425–458.
2. Agre, P., King, L. S., Yasui, M., Guggino, W. B., Ottersen, O. P., Fujiyoshi, Y. *et al.* (2002). Aquaporin water channels—from atomic structure to clinical medicine. *J. Physiol.* **542**, 3–16.
3. Gonen, T. & Walz, T. (2006). The structure of aquaporins. *Q. Rev. Biophys.* **39**, 361–396.
4. Törnroth-Horsefield, S., Wang, Y., Hedfalk, K., Johanson, U., Karlsson, M., Tajkhorshid, E. *et al.* (2006). Structural mechanism of plant aquaporin gating. *Nature*, **439**, 688–694.
5. Hedfalk, K., Törnroth-Horsefield, S., Nyblom, M., Johanson, U., Kjellbom, P. & Neutze, R. (2006). Aquaporin gating. *Curr. Opin. Struct. Biol.* **16**, 447–456.
6. Reichow, S. L. & Gonen, T. (2008). Noncanonical binding of calmodulin to aquaporin-0: implications for channel regulation. *Structure*, **16**, 1389–1398.
7. Landis, D. M. & Reese, T. S. (1974). Arrays of particles in freeze-fractured astrocytic membranes. *J. Cell Biol.* **60**, 316–320.
8. Rash, J. E., Yasumura, T., Hudson, C. S., Agre, P. & Nielsen, S. (1998). Direct immunogold labeling of aquaporin-4 in square arrays of astrocyte and ependymocyte plasma membranes in rat brain and spinal cord. *Proc. Natl Acad. Sci. USA*, **95**, 11981–11986.
9. Furman, C. S., Gorelick-Feldman, D. A., Davidson, K. G. V., Yasumura, T., Neely, J. D., Agre, P. & Rash, J. E. (2003). Aquaporin-4 square array assembly: opposing actions of M1 and M23 isoforms. *Proc. Natl Acad. Sci. USA*, **100**, 13609–13614.
10. Suzuki, H., Nishikawa, K., Hiroaki, Y. & Fujiyoshi, Y. (2008). Formation of aquaporin-4 arrays is inhibited by palmitoylation of N-terminal cysteine residues. *Biochim. Biophys. Acta*, **1778**, 1181–1189.
11. Zelenina, M., Zelenin, S., Bondar, A. A., Brismar, H. & Aperia, A. (2002). Water permeability of aquaporin-4 is decreased by protein kinase C and dopamine. *Am. J. Physiol. Renal Physiol.* **283**, F309–F318.
12. Han, Z., Wax, M. B. & Patil, R. V. (1998). Regulation of aquaporin-4 water channels by phorbol ester-dependent protein phosphorylation. *J. Biol. Chem.* **273**, 6001–6004.
13. Gunnarson, E., Axehult, G., Baturina, G., Zelenin, S., Zelenina, M. & Aperia, A. (2005). Lead induces increased water permeability in astrocytes expressing aquaporin 4. *Neuroscience*, **136**, 105–114.
14. Gunnarson, E., Zelenina, M., Axehult, G., Song, Y., Bondar, A., Krieger, P. *et al.* (2008). Identification of a molecular target for glutamate regulation of astrocyte water permeability. *Glia*, **56**, 587–596.
15. Silberstein, C., Bouley, R., Huang, Y., Fang, P., Pastor-Soler, N., Brown, D. & Van Hoek, A. N. (2004). Membrane organization and function of M1 and M23 isoforms of aquaporin-4 in epithelial cells. *Am. J. Physiol. Renal Physiol.* **287**, F501–F511.
16. Kadohira, I., Abe, Y., Nuriya, M., Sano, K., Tsuji, S., Arimitsu, T. *et al.* (2008). Phosphorylation in the C-terminal domain of aquaporin-4 is required for Golgi transition in primary cultured astrocytes. *Biochem. Biophys. Res. Commun.* **377**, 463–468.
17. Amiry-Moghaddam, M. & Ottersen, O. P. (2003). The molecular basis of water transport in the brain. *Nat. Rev. Neurosci.* **4**, 991–1001.
18. Papadopoulos, M. C. & Verkman, A. S. (2007). Aquaporin-4 and brain edema. *Pediatr. Nephrol.* **22**, 778–784.
19. Lennon, V. A., Kryzer, T. J., Pittock, S. J., Verkman, A. S. & Hinson, S. R. (2005). IgG marker of optic–spinal multiple sclerosis binds to the aquaporin-4 water channel. *J. Exp. Med.* **202**, 473–477.
20. Tani, K., Mitsuma, T., Hiroaki, Y., Kamegawa, A., Nishikawa, K., Tanimura, Y. & Fujiyoshi, Y. (2009). Mechanism of aquaporin-4's fast and highly selective water conduction and proton exclusion. *J. Mol. Biol.* **389**, 694–706.
21. Hiroaki, Y., Tani, K., Kamegawa, A., Gyobu, N., Nishikawa, K., Suzuki, H. *et al.* (2006). Implications of the aquaporin-4 structure on array formation and cell adhesion. *J. Mol. Biol.* **355**, 628–639.
22. Fischer, G., Kosinska-Eriksson, U., Aponte-Santamaria, C., Palmgren, M., Geijer, C., Hedfalk, K. *et al.* (2009). Crystal structure of a yeast aquaporin at 1.15 angstrom reveals a novel gating mechanism. *PLoS Biol.* **7**, e1000130.
23. Zhang, X., Ji, Y., Zhang, L., Harrison, S. C., Marinescu, D. C., Nibert, M. L. & Baker, T. S. (2005). Features of reovirus outer capsid protein mu1 revealed by electron cryomicroscopy and image reconstruction of the virion at 7.0 angstrom resolution. *Structure*, **13**, 1545–1557.
24. Appel, M., Hizlan, D., Vinothkumar, K. R., Ziegler, C. & Kuhlbrandt, W. (2009). Conformations of NhaA, the Na^+/H^+ exchanger from *Escherichia coli*, in the pH-activated and ion-translocating states. *J. Mol. Biol.* **388**, 659–672.
25. Ho, J. D., Yeh, R., Sandstrom, A., Chorny, I., Harries, W. E. C., Robbins, R. A. *et al.* (2009). Crystal structure of human aquaporin 4 at 1.8 Å and its mechanism of conductance. *Proc. Natl Acad. Sci. USA*, **106**, 7437–7442.
26. Smart, O. S., Neduvelil, J. G., Wang, X., Wallace, B. A. & Sansom, M. S. (1996). HOLE: a program for the analysis of the pore dimensions of ion channel structural models. *J. Mol. Graphics*, **14**, 354–360.
27. Sui, H., Han, B. G., Lee, J. K., Walian, P. & Jap, B. K. (2001). Structural basis of water-specific transport through the AQP1 water channel. *Nature*, **414**, 872–878.
28. Henderson, R., Baldwin, J. M., Downing, K. H., Lepault, J. & Zemlin, F. (1986). Structure of purple membrane from *Halobacterium halobium*: recording, measurement and evaluation of electron micrographs at 3.5 Å resolution. *Ultramicroscopy*, **19**, 147–178.
29. Nyblom, M., Frick, A., Wang, Y., Ekvall, M., Hallgren, K., Hedfalk, K. *et al.* (2009). Structural and functional

analysis of SoPIP2;1 mutants adds insight into plant aquaporin gating. *J. Mol. Biol.* **387**, 653–668.
30. Connell-Crowley, L., Solomon, M. J., Wei, N. & Harper, J. W. (1993). Phosphorylation independent activation of human cyclin-dependent kinase 2 by cyclin A *in vitro*. *Mol. Biol. Cell*, **4**, 79–92.
31. Groban, E. S., Narayanan, A. & Jacobson, M. P. (2006). Conformational changes in protein loops and helices induced by post-translational phosphorylation. *PLoS Comput. Biol.* **e32**, 2.
32. Narayanan, A. & Jacobson, M. P. (2009). Computational studies of protein regulation by post-translational phosphorylation. *Curr. Opin. Struct. Biol.* **19**, 156–163.
33. Murakami, S., Nakashima, R., Yamashita, E. & Yamaguchi, A. (2002). Crystal structure of bacterial multidrug efflux transporter AcrB. *Nature*, **419**, 587–593.
34. Murakami, S., Nakashima, R., Yamashita, E., Matsumoto, T. & Yamaguchi, A. (2006). Crystal structures of a multidrug transporter reveal a functionally rotating mechanism. *Nature*, **443**, 173–179.
35. Yukutake, Y., Tsuji, S., Hirano, Y., Adachi, T., Takahashi, T., Fujihara, K. *et al.* (2008). Mercury chloride decreases the water permeability of aquaporin-4-reconstituted proteoliposomes. *Biol. Cell*, **100**, 355–363.
36. Savage, D. F. & Stroud, R. M. (2007). Structural basis of aquaporin inhibition by mercury. *J. Mol. Biol.* **368**, 607–617.
37. Sorani, M. D., Zador, Z., Hurowitz, E., Yan, D., Giacomini, K. M. & Manley, G. T. (2008). Novel variants in human aquaporin-4 reduce cellular water permeability. *Hum. Mol. Genet.* **17**, 2379–2389.
38. Matthews, B. W. (1968). Solvent content of protein crystals. *J. Mol. Biol.* **33**, 491–497.
39. Crane, J. M., Van Hoek, A. N., Skach, W. R. & Verkman, A. S. (2008). Aquaporin-4 dynamics in orthogonal arrays in live cells visualized by quantum dot single particle tracking. *Mol. Biol. Cell*, **19**, 3369–3378.
40. Crane, J. M. & Verkman, A. S. (2009). Determinants of aquaporin-4 assembly in orthogonal arrays revealed by live-cell single-molecule fluorescence imaging. *J. Cell Sci.* **122**, 813–821.
41. Crane, J. M. & Verkman, A. S. (2009). Reversible, temperature-dependent supramolecular assembly of aquaporin-4 orthogonal arrays in live cell membranes. *Biophys. J.* **97**, 3010–3018.
42. Tajima, M., Crane, J. M. & Verkman, A. S. (2010). Aquaporin-4 associations and array dynamics probed by photobleaching and single-molecule analysis of GFP-AQP4 chimeras. *J. Biol. Chem.* **285**, 8163–8170.
43. Crowther, R. A., Henderson, R. & Smith, J. M. (1996). MRC image processing programs. *J. Struct. Biol.* **116**, 9–16.
44. Tani, K., Sasabe, H. & Toyoshima, C. (1996). A set of computer programs for determining defocus and astigmatism in electron images. *Ultramicroscopy*, **65**, 31–44.
45. Yakata, K., Hiroaki, Y., Ishibashi, K., Sohara, E., Sasaki, S., Mitsuoka, K. & Fujiyoshi, Y. (2007). Aquaporin-11 containing a divergent NPA motif has normal water channel activity. *Biochim. Biophys. Acta*, **1768**, 688–693.
46. Tanimura, Y., Hiroaki, Y. & Fujiyoshi, Y. (2009). Acetazolamide reversibly inhibits water conduction by aquaporin-4. *J. Struct. Biol.* **166**, 16–21.
47. Doi, T., Hiroaki, Y., Arimoto, I., Fujiyoshi, Y., Okamoto, T., Satoh, M. & Furuichi, Y. (1997). Characterization of human endothelin B receptor and mutant receptors expressed in insect cells. *Eur. J. Biochem.* **248**, 139–148.
48. Zeidel, M. L., Ambudkar, S. V., Smith, B. L. & Agre, P. (1992). Reconstitution of functional water channels in liposomes containing purified red cell CHIP28 protein. *Biochemistry*, **31**, 7436–7440.
49. van Heeswijk, M. P. & van Os, C. H. (1986). Osmotic water permeabilities of brush border and basolateral membrane vesicles from rat renal cortex and small intestine. *J. Membr. Biol.* **92**, 183–193.
50. Liu, R. & Persson, A. E. G. (2005). Simultaneous changes of cell volume and cytosolic calcium concentration in macula densa cells caused by alterations of luminal NaCl concentration. *J. Physiol.* **563**, 895–901.
51. Komlosi, P., Fintha, A. & Bell, P. D. (2006). Unraveling the relationship between macula densa cell volume and luminal solute concentration/osmolality. *Kidney Int.* **70**, 865–871.
52. Hibino, H. & Kurachi, Y. (2007). Distinct detergent-resistant membrane microdomains (lipid rafts) respectively harvest K^+ and water transport systems in brain astroglia. *Eur. J. Neurosci.* **26**, 2539–2555.